HHS Public Access

Author manuscript

Biomacromolecules. Author manuscript; available in PMC 2019 March 22.

Published in final edited form as:

Biomacromolecules. 2014 January 13; 15(1): 122–131. doi:10.1021/bm401406e.

Conformational Distribution and α-Helix to β-Sheet Transition of Human Amylin Fragment Dimer

Ruxi Qi[†], **Yin Luo**[†], **Buyong Ma**[‡], **Ruth Nussinov**[‡,§], and **Guanghong Wei**[†]

[†]State Key Laboratory of Surface Physics, Key Laboratory for Computational Physical Sciences (MOE), and Department of Physics, Fudan University, Shanghai, China

[‡]Basic Science Program, Leidos Biomedical Research, Inc., Cancer and Inflammation Program, NCI, Frederick, Maryland 21702, United States

[§]Sackler Inst. of Molecular Medicine Department of Human Genetics and Molecular Medicine Sackler School of Medicine, Tel Aviv University, Tel Aviv 69978, Israel

Abstract

Experiments suggested that the fibrillation of the 11–25 fragment (hIAPP(11–25)) of human islet amyloid polypeptide (hIAPP or amylin) involves the formation of transient α-helical intermediates, followed by conversion to β-sheet-rich structure. However, atomic details of α-helical intermediates and the transition mechanism are mostly unknown. We investigated the structural properties of the monomer and dimer in atomistic detail by replica exchange molecular dynamics (REMD) simulations. Transient α-helical monomers and dimers were both observed in the REMD trajectories. Our calculated H^{α} chemical shifts based on the monomer REMD run are in agreement with the solution-state NMR experimental observations. Multiple 300 ns MD simulations at 310 K show that α-helix-to-β-sheet transition follows two mechanisms: the first involved direct transition of the random coil part of the helical conformation into antiparallel β-sheet, and in the second, the α-helical conformation unfolded and converted into antiparallel β-sheet. In both mechanisms, the α-helix-to-β-sheet transition occurred via random coil, and the transition was accompanied by an increase of interpeptide contacts. In addition, our REMD simulations revealed different temperature dependencies of helical and β-structures. Comparison with experimental data suggests that the propensity for hIAPP(11–25) to form α-helices and amyloid structures is concentration- and temperature-dependent.

Graphical Abstract

Supporting Information

Additional data provided, including six figures. These figures present the starting conformation and convergence check of the REMD run of hIAPP(11–25) dimer, dwell time distributions of the REMD run of hIAPP(11–25) dimer, center conformations of the first eight most-populated clusters of hIAPP(11–25) dimer at 310 K, and the analysis of a representative helix-to-β-sheet transition pathway following mechanism I: a direct transition of the random coil part of the initial helical conformation into an antiparallel β-sheet and PMF using (R_g, RMSD) as reaction coordinates with representative structures. This material is available free of charge via the Internet at http://pubs.acs.org.

The authors declare no competing financial interest.

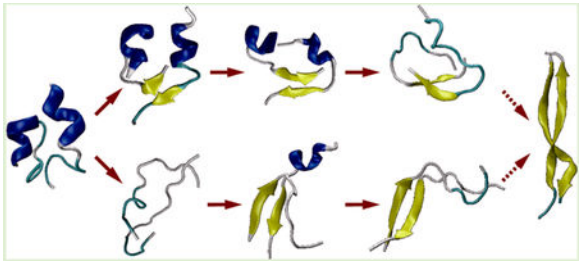

INTRODUCTION

The pathological self-assembly of proteins or peptides into highly ordered amyloid fibrils is associated with a number of human diseases such as type II diabetes Mellitus (T2DM), Alzheimer's disease, and Parkinson's disease.[1–3] In the T2DM, the main component of the amyloid deposits found in the pancreas has been identified as human islet amyloid polypeptide (hIAPP or amylin), a 37-residue peptide cosecreted with insulin by islet β-cells.[4,5] It has been proposed initially that fibril formation is responsible for the onset of T2DM due to the widespread observation of fibrils in post mortem evaluations of T2DM patients and in studies where synthetic hIAPP was applied to β-cell cultures.[6,7] However, growing evidence supports that soluble oligomers preceding the formation of fibrils are the major causative agents leading to β-cell death in type II diabetes.[7–11] Thus, exploring the oligomeric structures and the conformational dynamics in the process of hIAPP fibrillation is of great significance both for understanding the aggregation mechanism and designing therapeutic strategies. Yet until now the atomic details of oligomers formed in the early stage of aggregation remain poorly understood.[12] NMR spectroscopic studies on full-length IAPP peptide revealed a helical conformation of hIAPP and rat-IAPP.[13,14] The nature of hIAPP toxic species is still under discussion. For example, while β-sheet structure is usually more toxic, the membrane-disrupting hIAPP oligomers may be α-helix-rich[15,16] and may have toxic cell-penetrating peptide (CPP) properties.[17] Intriguingly, it has been shown that a single mutation of IAPP can diminish the toxicity in the N-terminal region.[18–20] Experimental studies have also explored the membrane perturbation effect by IAPP and its 20–29 fragment[21–23] with the aim of elucidating the membrane disruption and toxicity mechanism. In a recent review by Ramamoorthy and his co-workers, membrane disruption and early events in hIAPP aggregation have been discussed in detail.[24] However, complex behavior of hIAPP aggregates still strongly hampers a rational design of amyloid inhibitors.[25]

Substantial experimental investigations have been performed in the past several years to elucidate the molecular mechanism of hIAPP aggregation. Recent NMR studies showed that IAPP fibrillizes without an appreciable buildup of nonfibrillar intermediates,[26] and the large oligomeric species may be an off-pathway intermediate.[27] However, a number of experimental studies suggested that transient α-helical intermediates are involved in the process of hIAPP aggregation both in aqueous solution[28–31] and in membrane environment.[15,32,33] More recently, using limited proteolysis combined with mass spectrometry, Liu et al. identified that the 11–25 fragment of hIAPP was involved in the initial intermolecular interactions of full-length hIAPP.[34] By use of circular dichroism (CD), Fourier transform

infrared (FTIR), and NMR spectroscopies, they investigated the conformational changes of this hIAPP(11–25) segment and proposed that the fibrillation process of hIAPP(11–25) involves the formation of transient α-helix-rich intermediate in the lag phase, followed by a slow conversion to β-sheets.[34] Their further experimental studies strengthened the existence of α-helical intermediates in amyloid formation of hIAPP(11–25) and full-length hIAPP peptides.[35,36]

Inspired by experimental work, a growing number of computational studies have been carried out to characterize the monomeric and oligomeric structures of hIAPP[37–43] and different hIAPP fragments.[44–47] Although α-helical states are observed in some of those simulation studies, the conformational transition from α-helix to β-sheet is not well characterized. Recently, using metadynamics and bias-exchange simulations as well as transition path sampling simulations, Singh et al.[48] reported that the α-helical conformer of amylin monomer undergoes a transformation into the β-hairpin structure through either an ordered zipping mechanism or an unstructured coil intermediate. However, the mechanism for α-helix to β-sheet transition of hIAPP oligomers at atomic level remains to be determined.

As more general important phenomena, α-helical intermediates were also observed in the aggregation process of other amyloid peptides by experimental and computational studies, such as amyloid β-protein (Aβ)[49–52] and huntingtin N-terminal fragments (httNT).[53] Conversion of α-helix into β-sheet has been frequently observed in the process of amyloid formation, as in the case of the native insulin[54] and other designed peptides.[55] In the unfolding processes of β_2-microglobulin and two related variants (one with N-terminal hexapeptide deletion ΔN6 and the other with Lys57–Asp58 cleavage) studied by high-temperature molecular dynamics (MD) simulations, one observed the β-strand to α-helix transition, a process thought to be on pathway to the eventual amyloid formation of β_2-microglobulin.[56] In addition, in a recent study of an FF domain amyloid formation, Castillo, Chiti, and Ventura found an overlap between the propensity to form native α-helices and the propensity to form amyloid structures in protein segments, supporting the view that proteins use stable α-helices as a strategy to neutralize amyloidogenic stretches of proteins since proteins cannot avoid the presence of aggregation-prone regions.[57]

In this study, we investigated in atomistic level detail the monomeric and dimeric structures of the hIAPP(11–25) peptide by performing REMD[58] simulations. Transient α-helical states of the hIAPP(11–25) monomer and dimer were observed in REMD trajectories. Subsequently, we examined the transition of REMD-generated α-helical dimer to β-sheet structure by conventional MD simulations at 310 K. The conformational transition was found to take place through the increase of peptide–peptide interactions initiated by helix–helix association, followed either by the direct formation of β-sheet in the nonhelical region or by helix unfolding into random coil and then β-sheet. In addition, our REMD simulations reveal different temperature dependencies of helical and β-structures. Comparison of our simulation results with previous experimental data[34] suggests that the overlap between the propensity for hIAPP(11–25) to form α-helices and amyloid structures is concentration- and temperature-dependent, reflecting the overall optimization of protein properties.

MATERIALS AND METHODS

hIAPP(11–25) Monomer and Dimer Systems.

The hIAPP(11–25) peptide consists of 15 residues, with the amino acid sequence of RLANFLVHSSNNFGA, capped by the ACE (CH_3CO) group at the N-terminus and NH_2 group at the C-terminus, as done experimentally.[34] To mimic the experimental acidic pH condition (around pH 4.3),[34] the side chains of Lys and His were protonated (Lys^+, His^+), thus, the peptide carries two net positive charges. Initially the peptide is fully extended in both the monomer and the dimer systems. The two peptide chains in the dimer system are in a cross orientation with a minimum distance of 0.8 nm. The initial configuration of the hIAPP(11–25) dimer is shown in Figure S1 in the Supporting Information. The monomer and dimer systems were fully solvated with TIP4P[59] water molecules in a cubic box with a size of $5 \times 5 \times 5$ nm^3. Counterions (Cl^-) were added to neutralize the system. There are 4025 water molecules in monomer system and 3939 water molecules in dimer system. The final peptide concentration is 13.3 mM for monomer and 26.6 mM for dimer system. The concentration used here is 2 orders of magnitude higher than that used in far-UV CD and NMR experiments (133 μM).[34] This millimolar concentration, used in many simulations,[60–62] is higher than the experimental concentrations on the order of micromolar[34,63] but enables us to characterize the conformational ensembles from simulations using current computer facilities. A recent computational study on the oligomerization of the VEALYL peptide from insulin at four different concentrations (3.3, 8.3, 16.6, and 83 mM) showed that the final structures approached ordered aggregates with steric-zipper-like structural features, irrespective of the initial peptide concentration.[62]

REMD and MD Simulations.

All MD and REMD simulations were performed in the isothermal–isobaric (NPT) ensemble using GROMACS-4.5.3 software package[64,65] with OPLS-AA/L force field.[66] A previous computational study on two peptides showed that GROMOS96 overestimates the stability of the β conformation, and OPLS generates a better balance between α-helical and β-sheet structures.[67] In addition, a recent REMD study on Aβ(16–22) dimer and trimer showed that GROMOS96 favors β-sheet structures, and OPLS predicts diverse structures.[68] There are 44 replicas with temperatures ranging from 310 to 452 K for the monomer system and from 310 to 453 K for the dimer system, prepared using an approach reported previously.[69] The average acceptance ratios for both systems are 23%. Bond length of peptides and water molecules were constrained, respectively, using the LINCS[70] and SETTLE algorithms, allowing an integration time step of 2 fs. Nonbonded pair lists were updated every five integration steps. The protein and nonprotein (water and counterion) groups were separately coupled to an external heat bath with a relaxation time of 0.1 ps using a velocity rescaling coupling method.[71] The pressure was kept at 1 bar using the Parrinello-Rahman method[72] with a coupling time constant of 1.0 ps. Electrostatic interactions were treated with the particle mesh Ewald method with a real space cutoff of 1.0 nm. The van der Waals interactions were calculated using a cutoff of 1.4 nm. The exchange between two adjacent replicas was attempted every 1000 integration steps. The simulation time per replica is 200 ns for monomer and 300 ns for dimer.

Forty independent 300 ns MD simulations were performed to examine whether a hIAPP(11–25) helical dimer can transit into a β-sheet structure or not. The initial helical dimer was taken from dimer conformations generated in REMD run at 355 K. The forty MD runs started from the same initial helical dimer but with different random velocities. The system contains 3951 water molecules.

Analysis.

Trajectory analysis was performed with our in-house-developed codes and the facilities from GROMACS-4.5.3 software package.[64,65] The data in the first 30 and 50 ns REMD trajectories were discarded to remove the bias of the initial states for monomer and dimer, respectively. Continuous trajectories of the REMD run were produced using the demux tool from the GROMACS package. The secondary structure of the peptide conformation was identified using the DSSP program.[73] Structural analysis was performed using a main chain root-mean-square deviation (RMSD) cluster analysis method. The Daura method[74] was used to cluster the conformations sampled in the REMD simulations with a RMSD cutoff of 0.2 nm both for monomer and dimer using residues L12-G24, with R11 and A25 being excluded due to their high flexibilities. The chain-independent RMSD was calculated by completely neglecting the chain identifier in the coordinate file of the hIAPP(11–25) dimer to obtain the smallest RMSD as the two chains are topologically identical.[75] The two-dimensional (2D) free energy surface is constructed using $-RT \log P(R_g$, H-bond number), where $P(R_g$, H-bond number) is the probability of a conformation having a certain value of R_g and H-bond number. Here, R_g and H-bond number denote the radius of gyration of the dimer and the total number of hydrogen bonds (including intra- and intermolecular H-bonds), respectively. A H-bond is considered as formed if the N···O distance is less than 0.35 nm and the N–H···O angle is greater than 150°. The interpeptide interactions are analyzed by the probability of residue–residue contact maps. Here, a contact is defined when the aliphatic carbon atoms of two nonsequential side chains (or main chains) come within 0.54 nm or any other atoms of two nonsequential side chains (or main chains) lie within 0.46 nm. The VMD program[76] was used for trajectory visualization and for graphical structure analysis. H^{α} chemical shifts were calculated using the program SPARTA+.[77]

RESULTS

Converged REMD Simulations Reproduced NMR Chemical Shifts.

In order to examine the convergence and accuracy of the REMD simulations, we first examine the H^{α} chemical shifts of each amino acid residue in the hIAPP(11–25) monomer, for which solution NMR data are available.[34] Based on the 200 ns REMD simulation of the monomer system, the H^{α} chemical shifts of each amino acid residue were calculated for all the conformations generated within 30–200 ns, using the program SPARTA+.[77] As shown in Figure 1a,b, we essentially reproduced the experimental H^{α} chemical shifts. The calculated H^{α} secondary chemical shifts are also in agreement with the solution state NMR experimental observations, with a Pearson correlation coefficient of 0.57. Negative H^{α} secondary chemical shifts indicate a helical structure. Figure 1c,d shows representative REMD-generated helical and β structures of hIAPP(11–25) monomers in solution at 310 K. It can be seen that, in helical conformations, the N-terminal residues have a high propensity

to adopt helical structure (see below for more detailed discussion), while β conformations mainly populate hairpin-like structures.

The convergence of the REMD run for the dimer was checked using the probability distributions of R_g generated within two independent time intervals: 50–175 and 175–;300 ns. As seen from Figure S2(a), the two probability distribution curves overlap very well, indicating a good convergence of REMD simulations. We also monitored the time evolution of replicas by tracing one replica (replica 1) in temperature space. The time evolution of replica 1 shows that the peptide visited sufficiently the entire temperature space (see Figure S2(b)). In addition, we calculated the percentage of dwell time at each temperature for each of the 44 replicas (Figure S3). Each of the 44 replicas samples all of the 44 temperatures through the 300 ns simulation time, indicating sufficient sampling. The overall standard deviations also show an appropriate sampling of the REMD simulation. These results demonstrate that our REMD simulations reasonably converged for both monomer and dimer systems.

hIAPP(11–25) Dimer Displays Much Higher β-Sheet Propensity than Monomer.

To further study the conformational properties, we calculated the secondary structure distributions of monomers and dimers at 310 K (Figure 2). Structural analysis was performed using a RMSD-based cluster analysis described in Materials and Methods. Using a cutoff of 0.2 nm, we separated the monomer conformations into 180 clusters. It can be seen from Figure 2 that the monomer adopts mainly random coil conformations with a high percentage of coil (~40%), bend (~30%), and turn (17%) and a low percentage of helix (6%) and β-sheet (7%). The 6% helix indicates that the helical structure is transiently populated, consistent with a recent solution-state NMR study on the hIAPP(11–25) monomer.[34]

We also performed structural analysis on the hIAPP(11–25) dimer. With a RMSD cutoff of 0.2 nm, the dimer conformations at 310 K were separated into 518 clusters. The center conformations of the first eight most-populated clusters are shown in Figure S4. This larger cluster number reflects that the structural diversity of the dimer is more pronounced than that of the monomer. However, the secondary structure propensities for the dimer conformers are more consistent. For example, even though all of these clusters display certain conformational disorder, most of them contain β-sheet content (except for clusters 3, 4, and 8). Figure 2 shows that, with respect to the monomer, the dimer displays a significantly increased β-content (23%) and a decreased turn content (7%), although the dimer mostly populates random coil states with a coil content of 43% and a bend content of 23%. Compared with monomers (6% for helix and 7% for β-sheet), dimers have relatively lower probability to adopt helical conformations (3%), while they have a significantly higher probability to adopt β-conformations (23%).

To obtain residue-specific α-helix and β-sheet propensities, we calculated the secondary structure probability as a function of the amino acid residue. As shown in Figure 3, both monomers and dimers have a propensity to sample helical structures in the N-terminal region spanning residues A13–V17, and sample β-sheet conformation both in the N- and C-terminal regions. Monomers have slightly higher probability to adopt helical structures than dimers, whereas dimers have significantly higher probability to sample β-structures.

We further investigated the percentage of β-sheet and helix content as a function of temperature, both for monomer and dimer. Different temperature dependencies were observed (Figure 4). For both systems, the probability of β-structure decreases monotonically with increasing temperature, whereas the probability of helical structure has a wide peak with an initial slow increment and then a gradual decline. This indicates that helical and β-structures have different temperature sensitivities. Similar phenomenon was observed previously in a REMD study of hIAPP pentapeptide (hIAPP(15–19)) aggregation, [46] which reveals a generality of such a kind of temperature dependence of certain peptide sequences. In short, our REMD results indicate that the α-helix and β-sheet propensities of hIAPP(11–25) are concentration- and temperature-dependent.

Coexistence of α-Helix- and β-Sheet-Rich Conformers in the Global Minimum of Free Energy Surface of hIAPP(11–25) Dimer.

The conformational properties of hIAPP(11–25) monomer and dimer can be effectively characterized by the radius of gyration and the number of main-chain hydrogen bonds. The average R_g per chain is 0.72 nm in the monomer and 0.87 nm in the dimer, indicating that the hIAPP(11–25) peptide chain in the dimer system has a slightly larger dimension than in the monomer system. We probed the intrapeptide stabilization by computing the average number of intrapeptide hydrogen bonds per chain. The value is 2.85 for monomer and 0.6 for dimer. The presence of a relatively larger number of intrapeptide H-bonds in the monomer system reflects the formation of helical or β-sheet structures. Although the average number of intrapeptide H-bonds in the dimer system is less than 1, the total number of H-bonds is much larger (~8) when interpeptide H-bonds are included.

To have an overall view of the conformational distribution of hIAPP(11–25) dimer, we constructed the 2D free energy surface (or potential of mean force, PMF) in Figure 5 using $-RT\log P(R_g$, H-bond number) described in Analysis. As shown in Figure 5, the free energy surface contains three minimum-energy basins, centered at (R_g, H-bond number) values of (0.85 nm, 8), (1.12 nm, 10), and (1.33 nm, 11). The deepest basin at (0.85 nm, 8) is populated by multiple conformations, mainly corresponding to collapsed and disordered states with helix, β-sheet, and random coil contents (see snapshots, Figure 5A–D). The basins located at (1.12 nm, 10) and (1.33 nm, 11) are rather shallow, corresponding to relatively extended states with high β-sheet content. The β-sheet structures found in these minimum-energy basins are mostly antiparallel (see snapshots, Figure 5E–H).

The PMF features described above reveal two important characteristics of the free energy surface of the hIAPP(11–25) dimer. First, the barriers among the three energy basins are relatively low, indicating that easy conversion can occur among the conformers between two adjacent energy basins. The second characteristic is that the α-helical structure was observed to coexist with random coil and disordered β-sheet-rich conformers in the global minimum-energy basin. This observation implies that conformational transition among α-helical, random coil, and β-sheet-rich conformers may take place readily. When tracing one replica through temperature space, we found a long-enduring stable α-helical conformation. This finding, together with the two PMF features, suggests the existence of an α-helix-rich intermediate and the possibility of α-helix to β-sheet transition of the hIAPP(11–25) dimer.

We note that the observed low energy barrier in the 2D free energy surface here depends on the reaction coordinates used as certain reaction coordinates can only reflect limited features of a high-dimensional free energy landscape. To have another view of the free energy landscape, we also plotted the 2D freee energy surface using (R_g, RMSD) as reaction coordinates (Figure S6). Consistently, we found that the energy barriers from extended conformations to compact ones are relatively low.

To better understand the roles of different residues in the formation of dimeric structures, we re-examine the details of the peptide–peptide interactions from the probability of interpeptide contacts between all pairs of residues of the hIAPP(11–25) dimer from the REMD run. We see from Figure 6 that the pairwise contact probabilities among hydrophobic residues L12, A13, F15, L16, V17, and Phe23 are relatively higher than others, indicating that hydrophobic interaction plays a considerable role in hIAPP(11–25) dimerization. The importance of hydrophobic interactions to the dimerization of hIAPP(11–25) is consistent with recent experimental studies on the amyloid formation of the 20–29[78] and 22–29[79] fragments of hIAPP. The role of aromatic stacking interactions in the amyloid formation of hIAPP and/or its fragment is under debate.[78–81] Some studies suggested that an aromatic residue is not required for amyloid formation,[78,81] while other studies reported that aromatic–aromatic interaction play a negligible role in amyloid formation.[79,80] In our current study, we observed limited Phe-Phe interactions. As can be seen in Figure 6, the highest contact probabilities come from A13-F23 and F15–N22 contacts, indicating that hydrophobicity is more important than direct aromatic stacking to the dimerization of hIAPP(11–25) peptide.

Conformational Transition of hIAPP(11–25) Dimer from α-Helix to β-Sheet Occurred through Random Coil States.

To examine whether structural transition from α-helix to β-sheet can take place in the dimerization process of the hIAPP(11–25) peptide, we carried out forty 300-ns independent MD simulations using different initial velocity distributions in the NPT ensemble at 310 K. The starting conformation of those MD runs is a helical dimer taken from the replica at 355 K, very close to snapshot B in Figure 5 (with a main-chain RMSD of 0.18 nm). Conformational transition from α-helix to β-sheet was observed in 9 out of 40 MD runs. We characterized these MD trajectories by calculating the number of main-chain H-bonds, interpeptide contact number, and peptide main-chain RMSD with respect to the β-sheet part of the conformation at 150 ns. We found that the transition took place through two different mechanisms (denoted as I and II), which are illustrated in Figures 7 and 8. The detailed analysis of a representative helix-to-β-sheet transition pathway following mechanism I is given in Figure 7. We see that the random coil part of the initial helical conformation directly transited into a short antiparallel β-sheet at t = 26 ns (Figure 7a,b), during which the total number of H-bonds changed slightly (Figure 7c). This β-sheet structure was maintained in the remainder of the MD trajectory (with a RMSD < 0.2 nm relative to the β-sheet formed at 150 ns; Figure 7d). The formation and stabilization of this β-sheet structure weakened the helix–helix association (see the snapshot at t = 130 ns) and a complete unfolding of the helical structure was observed at t = 263 ns. This helix-to-β-sheet transition was

accompanied by the increase in the number of interpeptide contacts (Figure 7e). Eight MD trajectories follow this transition mechanism (a similar MD trajectory is given in Figure S5).

Figure 8 presents the detailed analysis of the helix-to-β-sheet transition pathway following mechanism II. It can be seen from Figure 8a,b that the initial helical conformation unfolded after 50 ns and transited into a random coil structure at t = 100 ns. The process of helix unfolding was accompanied by a decrease in the number of H-bonds within the first 100 ns (Figure 8c). Afterward, the number of H-bonds started to increase and a transition from random coil to a short antiparallel β-sheet structure occurred at t = 127 ns (Figure 8a). This short β-sheet structure remained stable in this MD trajectory (with a RMSD < 0.2 nm with respect to the β-sheet formed at 150 ns; Figure 8d) and it became longer at t = 270 ns. We expect that this partially formed antiparallel β-sheet would elongate with simulation time and become a fully extended antiparallel β-sheet (like snapshot H in Figure 5) if the simulation time is long enough. Interestingly, the process of helix unfolding and helix-to-β-sheet transition was accompanied by an increase in the number of interpeptide contacts (Figure 8e). Similarly, in other MD runs, the number of interpeptide contacts also increased during the formation of β-sheets (see Figures 7 and S5). Results from these MD simulations suggest that the conformational transition of hIAPP(11–25) dimer from α-helical state to β-sheet takes place through an intermediate random coil state and is facilitated by interpeptide interactions.

To reveal the physical interactions underlying the helix-to-sheet transition of the hIAPP(11–25) dimer, we probe the details of the peptide–peptide interactions before and after β-sheet formation. This can be estimated by the probability of interpeptide contacts between all pairs of residues in the hIAPP(11–25) dimer in the two representative MD runs shown in Figures 7 and 8. It can be seen from Figure 9 that the interpeptide N-terminal helix–helix (mostly hydrophobic) interactions and the pairwise contacts among the C-terminal residues N21, N22, F23, and G24 are prominent before β-sheet formation. After β-sheet was formed, the interpeptide N-terminal interactions disappeared or were reduced, while the interpeptide C-terminal residues interactions were preserved or enhanced, especially, those between N21–N22, N22–N22, N21–F23, and N22–F23 pairs. These results indicate that the initial helix–helix interactions and the C-terminal residues N21–F23 interactions play an important role in the random-coil-bridged helix-to-sheet transition and the β-sheet stabilization of hIAPP(11–25) dimer. Note that limited F23–F23 contacts are seen in the residue-based pairwise contact probability maps, indicating that the aromatic stacking interaction between F23–F23 is not so significant, consistent with the result from the REMD-generated contact probability map (Figure 6) of all conformations of hIAPP(11–25) dimer.

DISCUSSION

We investigated the structural properties of monomers and the smallest oligomers, that is, dimers of hIAPP(11−25) by performing extensive REMD simulations. We found that dimerization of hIAPP(11–25) led to a significant shift in the conformational propensities of the peptide. The average radius of gyration of a single peptide in a monomer and dimer increases from 0.72 to 0.87 nm, which indicates that peptides become more extended upon dimerization. Dimerization caused a decrease of the number of intrapeptide hydrogen bonds

per chain (from 2.85 to 0.6) and an increase of the number of interpeptide hydrogen bonds. More strikingly, the populations of secondary structure content in hIAPP(11–25) dimer undergo a drastic change with respect to the monomer. The average percentage of β-content increases from 7 to 23%, while that of α-helix decreases from 6 to 3%. We found that both monomers and dimers have a tendency for a helical conformation mainly in the N-terminal region, and for a β conformation in both the N- and C-terminal regions, indicating that the N-terminal region has the propensity for both α-helical and β-sheet structures. We also found that α-helical and β-sheet structures have different temperature dependencies. There are no specific α-helical stabilization regions in the free energy landscape of hIAPP(11–25) dimer (Figure 5).

Our extensive REMD simulation shows that monomeric hIAPP(11–25) is predominantly a random coil with a helical content of 6%, consistent with the previous solution-state ^{1}H NMR study which reported the presence of transient α-helical structure in the hIAPP(11–25) monomer.[34] This is also consistent with previous NMR studies of full-length IAPP monomer in aqueous solution, suggesting the presence of transient α-helices.[28]–[31] The CD spectroscopy of hIAPP(11–25) also suggested the assembly of monomers into α-helix-rich intermediates.[34] It is noted that in the solution-state ^{1}H NMR spectra, peaks due to intermediates including small oligomers were not observed during the aggregation of hIAPP(11–25) peptide,[34] indicative of fast dimerization process. Thus, the α-helix-rich intermediates observed in experiment are likely multimers larger than dimers. In this case the dimer result from our REMD simulations can not be compared directly with experiment. Our results showed that the propensity of helix and β-sheet is sensitive to monomeric and dimeric states, implying strong concentration dependence. Similar secondary structure shift was also observed for the monomers and dimers of Aβ(25–35)/Aβ by us[82] and by other groups.[83,84]

Multiple MD simulations were also carried out to examine the mechanism of α-helix to β-sheet transition of hIAPP(11–25) dimer. Helix-to-sheet transformation was observed in 9 out of forty 300-ns MD trajectories at 310 K. We found that the conformational transition occurred through two different mechanisms. The first mechanism involved a direct transition of the random coil part of the initial helical conformation into an antiparallel β-sheet. In the second mechanism, the initial α-helical conformation first unfolded to adopt a transient random coil conformation and then converted into an antiparallel β-sheet. In both mechanisms, α-helix-to-β-sheet transition occurred via a random coil state and the transition was companied by an increase in the number of interpeptide atomic contacts. Here the initial helix–helix interaction plays the role of a trigger, necessary for the conversion to β-sheets, by providing a higher chance for contact for the two peptides. The mechanism proposed here is consistent with previous experimental work suggesting that helical dimerization is on the pathway of fibril formation of full-length hIAPP.[85] In particular, the first mechanism observed here is similar to a recently reported helix-to-sheet transition mechanism of full-length hIAPP in solution at acidic pH.[40] Our simulations go, however, one step beyond by showing that following the coil-to-sheet transition, the helix part of the initial helical conformation unfolded to adopt an extended state. Our study suggests that the α-helix-rich conformation facilitates interpep-tide interactions, leading to the helix-to-β-sheet transition. Very recently, using REMD simulations with implicit solvent, Wu and Shea studied the

monomeric structures of full-length IAPP from four different species (human, rat, cat, and pig). Their simulations revealed that monomeric IAPP populates helix–coil, β-hairpin, and to a lesser extent helix-hairpin conformations. Consistent with their study, helix–coil and β-hairpin conformations were also observed in our REMD run for hIAPP(11–25) monomer. Based on the monomeric structural features of aggregating (human and cat) and nonaggregating (rat and pig) sequences, they speculated that the helix-hairpin conformation may act as an on-pathway intermediate leading to β-rich conformations.[43] Whether the helix-hairpin conformation is an on-pathway state to β-rich structure remains to be determined.

Moreover, of interest is the different temperature sensitivities of α-helical and β-structures. The helical content increases gradually with increasing temperature within a wide temperature range and ends in slow decrease, while the β-content decreases monotonically with increasing temperature. This feature was also observed previously in the pentapeptide hIAPP(15–19),[46] which reveals a generality of such kind of temperature dependence of certain peptide sequences. Indeed, this may provide some clues into the high temperature endurance of hyperthermophilic proteins, where the respective organisms thrive at temperatures near and even above 373 K.[86,87] The high-temperature-endurable ordered secondary structures, such as helices observed here, are essential to the exceedingly stable protein molecules. Therefore, the overlap between the α-helices and amyloid structures propensity in protein segments is concentration- and temperature-dependent, reflecting overall optimization of protein properties during evolution of protein sequences.

CONCLUSIONS

In this study, we have investigated the conformational ensemble and α-helix-to-β-sheet transition of the hIAPP(11–25) dimer by performing extensive REMD and MD simulations. Our REMD run on the hIAPP(11–25) monomer reproduced experimental observations of NMR chemical shifts. REMD run on dimers reveals the coexistence of α-helical dimers, β-sheet-rich conformations (including compact disordered β-sheet-rich dimers and fully extended antiparallel β-sheets), and random coil states. Secondary structure comparison between dimers and monomers shows that dimerization of hIAPP(11–25) resulted in a significant shift in the conformational propensities of the peptide. Monomers have slightly higher probability to adopt helical structures than dimers, whereas dimers have significantly higher probability to sample β-structures. In addition, our REMD simulations revealed different temperature dependencies of helical and β-structures. Results from multiple long MD simulations reveal that the conformational transition of hIAPP(11–25) dimer from an α-helical state to β-sheet structure occurred through an intermediate random coil state and it was accompanied by the increase of peptide–peptide atomic contacts. The formation of α-helices may kinetically facilitate the β-sheet formation by providing a compact nucleating contact, mostly through hydrophobic interactions in the N-terminal region. As the hIAPP(11–25) peptide was identified to be responsible for the initial intermolecular contacts in the aggregation of hIAPP, these results obtained from hIAPP(11–25) might provide structural insights into the transition mechanism between α-helix and β-sheet conformations of full-length hIAPP oligomers.

Supplementary Material

Refer to Web version on PubMed Central for supplementary material.

ACKNOWLEDGMENTS

G.W. acknowledges the financial support from the NSF of China (Grant Nos. 91227102, 11074047, and 11274075) and the Research Fund for the Doctoral Program of Higher Education of China. Simulations were performed at the Shanghai Supercomputing Center and the National High Performance Computing Center of Fudan University. This project has been funded in whole or in part with Federal funds from the National Cancer Institute, National Institutes of Health, under Contract No. HHSN261200800001E. This research was supported (in part) by the Intramural Research Program of the NIH, National Cancer Institute, Center for Cancer Research.

REFERENCES

(1). Kelly JW Curr. Opin. Struct. Biol 1998, 8, 101–106. [PubMed: 9519302]

(2). Rochet J-C; Lansbury PT, Jr. Curr. Opin. Struct. Biol 2000, 10, 60–68. [PubMed: 10679462]

(3). Clark A; Lewis CE; Willis AC; Cooper GJS; Morris JF; Reid KBM; Turner RC Lancet 1987, 330, 231–234.

(4). Cooper GJ; Willis AC; Clark A; Turner RC; Sim RB; Reid KB Proc. Natl. Acad. Sci. U.S.A 1987, 84, 8628–8632. [PubMed: 3317417]

(5). Westermark P; Wernstedt C; Wilander E; Hayden DW; O'Brien TD; Johnson KH Proc. Natl. Acad. Sci. U.S.A 1987, 84, 3881–3885. [PubMed: 3035556]

(6). Marzban L; Rhodes CJ; Steiner DF; Haataja L; Halban PA; Verchere CB Diabetes 2006, 55, 2192–2201. [PubMed: 16873681]

(7). Porat Y; Kolusheva S; Jelinek R; Gazit E Biochemistry 2003, 42, 10971–10977. [PubMed: 12974632]

(8). Hull RL; Westermark GT; Westermark P; Kahn SE J. Clin. Endocrinol. Metab 2004, 89, 3629–3643. [PubMed: 15292279]

(9). Hebda JA; Miranker AD Annu. Rev. Biophys 2009, 38, 125–152. [PubMed: 19416063]

(10). Jayasinghe SA; Langen R Biochim. Biophys. Acta, Biomembr 2007, 1768, 2002–2009.

(11). Haataja L; Gurlo T; Huang CJ; Butler PC Endocr. Rev 2008, 29, 303–316. [PubMed: 18314421]

(12). Cao P; Marek P; Noor H; Patsalo V; Tu L-H; Wang H; Abedini A; Raleigh DP FEBS Lett. 2013, 587, 1106–1118. [PubMed: 23380070]

(13). Nanga RPR; Brender JR; Xu J; Hartman K; Subramanian V; Ramamoorthy AJ Am. Chem. Soc 2009, 131, 8252–8261.

(14). Brender JR; Lee EL; Cavitt MA; Gafni A; Steel DG; Ramamoorthy AJ Am. Chem. Soc 2008, 130, 6424–9.

(15). Knight JD; Hebda JA; Miranker AD Biochemistry 2006, 45, 9496–9508. [PubMed: 16878984]

(16). Last NB; Rhoades E; Miranker AD Proc. Natl. Acad. Sci. U.S.A 2011, 108, 9460–9465. [PubMed: 21606325]

(17). Magzoub M; Miranker AD FASEB J. 2012, 26, 1228–1238. [PubMed: 22183778]

(18). Nanga RP; Brender JR; Xu J; Veglia G; Ramamoorthy A Biochemistry 2008, 47, 12689–97. [PubMed: 18989932]

(19). Brender JR; Hartman K; Reid KR; Kennedy RT; Ramamoorthy A Biochemistry 2008, 47, 12680–8. [PubMed: 18989933]

(20). Nanga RP; Brender JR; Vivekanandan S; Ramamoorthy A Biochim. Biophys. Acta 2011, 1808, 2337–42. [PubMed: 21723249]

(21). Sciacca MF; Brender JR; Lee DK; Ramamoorthy A Biochemistry 2012, 51, 7676–84. [PubMed: 22970795]

(22). Sciacca MF; Milardi D; Messina GM; Marletta G; Brender JR; Ramamoorthy A; La Rosa C Biophys. J 2013, 104, 173–84. [PubMed: 23332070]

(23). Brender JR; Heyl DL; Samisetti S; Kotler SA; Osborne JM; Pesaru RR; Ramamoorthy A Phys. Chem. Chem. Phys 2013, 15, 8908–15. [PubMed: 23493863]

(24). Brender JR; Salamekh S; Ramamoorthy A Acc. Chem. Res 2011, 45, 454–462. [PubMed: 21942864]

(25). Middleton CT; Marek P; Cao P; Chiu C.-c.; Singh S; Woys AM; de Pablo JJ; Raleigh DP; Zanni MT Nature Chem. 2012, 4, 355–360. [PubMed: 22522254]

(26). Suzuki Y; Brender JR; Hartman K; Ramamoorthy A; Marsh EN Biochemistry 2012, 51, 8154–62. [PubMed: 22998665]

(27). Soong R; Brender JR; Macdonald PM; Ramamoorthy AJ Am. Chem. Soc 2009, 131, 7079–85.

(28). Williamson JA; Miranker AD Protein Sci. 2007, 16, 110–117. [PubMed: 17123962]

(29). Yonemoto IT; Kroon GJ; Dyson HJ; Balch WE; Kelly JW Biochemistry 2008, 47, 9900–10. [PubMed: 18710262]

(30). Williamson JA; Loria JP; Miranker AD J. Mol. Biol 2009, 393, 383–396. [PubMed: 19647750]

(31). Cort JR; Liu Z; Lee GM; Huggins KNL; Janes S; Prickett K; Andersen NH Protein Eng., Des. Sel 2009, 22, 497–513. [PubMed: 19596697]

(32). Fu L; Liu J; Yan ECY J. Am. Chem. Soc 2011, 133, 8094–8097. [PubMed: 21534603]

(33). Jayasinghe SA; Langen R Biochemistry 2005, 44, 12113–12119. [PubMed: 16142909]

(34). Liu G; Prabhakar A; Aucoin D; Simon M; Sparks S; Robbins KJ; Sheen A; Petty SA; Lazo ND J. Am. Chem. Soc 2010, 132, 18223–18232. [PubMed: 21138275]

(35). Liu G; Robbins KJ; Sparks S; Selmani V; Bilides KM; Gomes EE; Lazo ND Biochemistry 2012, 51, 4167–74. [PubMed: 22559877]

(36). Sparks S; Liu G; Robbins KJ; Lazo ND Biochem. Biophys. Res. Commun 2012, 422, 551–555. [PubMed: 22579683]

(37). Dupuis NF; Wu C; Shea J-E; Bowers MT J. Am. Chem. Soc 2009, 131, 18283–18292. [PubMed: 19950949]

(38). Laghaei R; Mousseau N; Wei GJ Phys. Chem. B 2010, 114, 7071–7077.

(39). Reddy AS; Wang L; Singh S; Ling YL; Buchanan L; Zanni MT; Skinner JL; de Pablo JJ Biophys. J 2010, 99, 2208–2216. [PubMed: 20923655]

(40). Dupuis NF; Wu C; Shea J-E; Bowers MT J. Am. Chem. Soc 2011, 133, 7240–7243. [PubMed: 21517093]

(41). Laghaei R; Mousseau N; Wei GJ Phys. Chem. B 2011, 115, 3146–3154.

(42). Liang G; Zhao J; Yu X; Zheng J Biochemistry 2013, 52, 1089–1100. [PubMed: 23331123]

(43). Wu C; Shea JE PLoS Comput. Biol 2013, 9, e1003211. [PubMed: 24009497]

(44). Mo YX; Lu Y; Wei GH; Derreumaux PJ Chem. Phys 2009, 130.

(45). Jiang P; Xu W; Mu Y PLoS Comput. Biol 2009, 5, e1000357. [PubMed: 19360098]

(46). Singh G; Brovchenko I; Oleinikova A; Winter RJ Phys. Chem. B 2009, 113, 9863–9870.

(47). Xu W; Jiang P; Mu YJ Phys. Chem. B 2009, 113, 7308–7314.

(48). Singh S; Chiu C.-c.; Reddy AS; de Pablo JJ J. Chem. Phys 2013, 138, 155101–10. [PubMed: 23614446]

(49). Kirkitadze MD; Condron MM; Teplow DB J. Mol. Biol 2001, 312, 1103–1119. [PubMed: 11580253]

(50). Zhang T; Zhang J; Derreumaux P; Mu YJ Phys. Chem. B 2013, 117, 3993–4002.

(51). Chebaro Y; Jiang P; Zang T; Mu Y; Nguyen PH; Mousseau N; Derreumaux PJ Phys. Chem. B 2012, 116, 8412–22.

(52). Lin YS; Bowman GR; Beauchamp KA; Pande VS Biophys. J 2012, 102, 315–24. [PubMed: 22339868]

(53). Jayaraman M; Kodali R; Sahoo B; Thakur AK; Mayasundari A; Mishra R; Peterson CB; Wetzel RJ Mol. Biol 2012, 415, 881–899.

(54). Yamamoto S; Watarai H Chirality 2012, 24, 97–103. [PubMed: 22180158]

(55). Singh Y; Sharpe PC; Hoang HN; Lucke AJ; McDowall AW; Bottomley SP; Fairlie DP Chem.—Eur. J 2011, 17, 151–160. [PubMed: 21207612]

(56). Ma B; Nussinov R Protein Eng. 2003, 16, 561–575. [PubMed: 12968074]
(57). Castillo V; Chiti F; Ventura S PLoS One 2013, 8, e58297. [PubMed: 23505482]
(58). Sugita Y; Okamoto Y Chem. Phys. Lett 1999, 314, 141–151.
(59). Jorgensen WL; Chandrasekhar J; Madura JD; Impey RW; Klein ML J. Chem. Phys 1983, 79, 926–935.
(60). Gnanakaran S; Nussinov R; Garcia AE J. Am. Chem. Soc 2006, 128, 2158–9. [PubMed: 16478138]
(61). Nasica-Labouze J; Meli M; Derreumaux P; Colombo G; Mousseau N PLoS Comput. Biol 2011, 7, e1002051. [PubMed: 21625573]
(62). Matthes D; Gapsys V; de Groot BL J. Mol. Biol 2012, 421, 390–416. [PubMed: 22326493]
(63). Lu J-X; Qiang W; Yau W-M; Schwieters CD; Meredith SC; Tycko R Cell 2013, 154, 1257–1268. [PubMed: 24034249]
(64). Berendsen HJC; van der Spoel D; van Drunen R Comput. Phys. Commun 1995, 91, 43–56.
(65). Lindahl E; Hess B; van der Spoel DJ Mol. Model 2001, 7, 306–317.
(66). Kaminski GA; Friesner RA; Tirado-Rives J; Jorgensen WL J. Phys. Chem. B 2001, 105, 6474–6487.
(67). Yoda T; Sugita Y; Okamoto Y Chem. Phys. Lett 2004, 386, 460–467.
(68). Nguyen PH; Li MS; Derreumaux P Phys. Chem. Chem. Phys 2011, 13, 9778–88. [PubMed: 21487594]
(69). Patriksson A; van der Spoel D Phys. Chem. Chem. Phys 2008, 10, 2073–7. [PubMed: 18688361]
(70). Hess B; Bekker H; Berendsen HJC; Fraaije JG E. M. J. Comput. Chem 1997, 18, 1463–1472.
(71). Bussi G; Donadio D; Parrinello MJ Chem. Phys 2007, 126, 014101–7.
(72). Nosé S; Klein ML Mol. Phys 1983, 50, 1055–1076.
(73). Kabsch W; Sander C Biopolymers 1983, 22, 2577–2637. [PubMed: 6667333]
(74). Daura X; Gademann K; Jaun B; Seebach D; van Gunsteren WF; Mark AE Angew. Chem., Int. Ed 1999, 38, 236–240.
(75). Li H; Luo Y; Derreumaux P; Wei G Biophys. J 2011, 101, 2267–2276. [PubMed: 22067167]
(76). Humphrey W; Dalke A; Schulten KJ Mol. Graphics 1996, 14, 33–38.
(77). Shen Y; Bax AJ Biomol. NMR 2010, 48, 13–22.
(78). Doran TM; Kamens AJ; Byrnes NK; Nilsson BL Proteins: Struct., Funct., Bioinf 2012, 80, 1053–1065.
(79). Profit AA; Felsen V; Chinwong J; Mojica E-RE; Desamero RZB Proteins: Struct., Funct., Bioinf 2013, 81, 690–703.
(80). Gazit E FASEB J. 2002, 16, 77–83. [PubMed: 11772939]
(81). Tracz SM; Abedini A; Driscoll M; Raleigh DP Biochemistry 2004, 43, 15901–8. [PubMed: 15595845]
(82). Wei G; Jewett AI; Shea J-E Phys. Chem. Chem. Phys 2010, 12, 3622–3629. [PubMed: 20336261]
(83). Takeda T; Klimov DK Proteins: Struct., Funct., Bioinf 2009, 77, 1–13.
(84). Kim S; Takeda T; Klimov DK Biophys. J 2010, 99, 1949–58. [PubMed: 20858441]
(85). Wiltzius JJW; Sievers SA; Sawaya MR; Eisenberg D Protein Sci. 2009, 18, 1521–1530. [PubMed: 19475663]
(86). Blöchl E; Burggraf S; Fiala G; Lauerer G; Huber G; Huber R; Rachel R; Segerer A; Stetter KO; Völkl P World J. Microbiol. Biotechnol 1995, 11, 9–16. [PubMed: 24414408]
(87). Stetter KO FEBS Lett. 1999, 452, 22–25. [PubMed: 10376671]

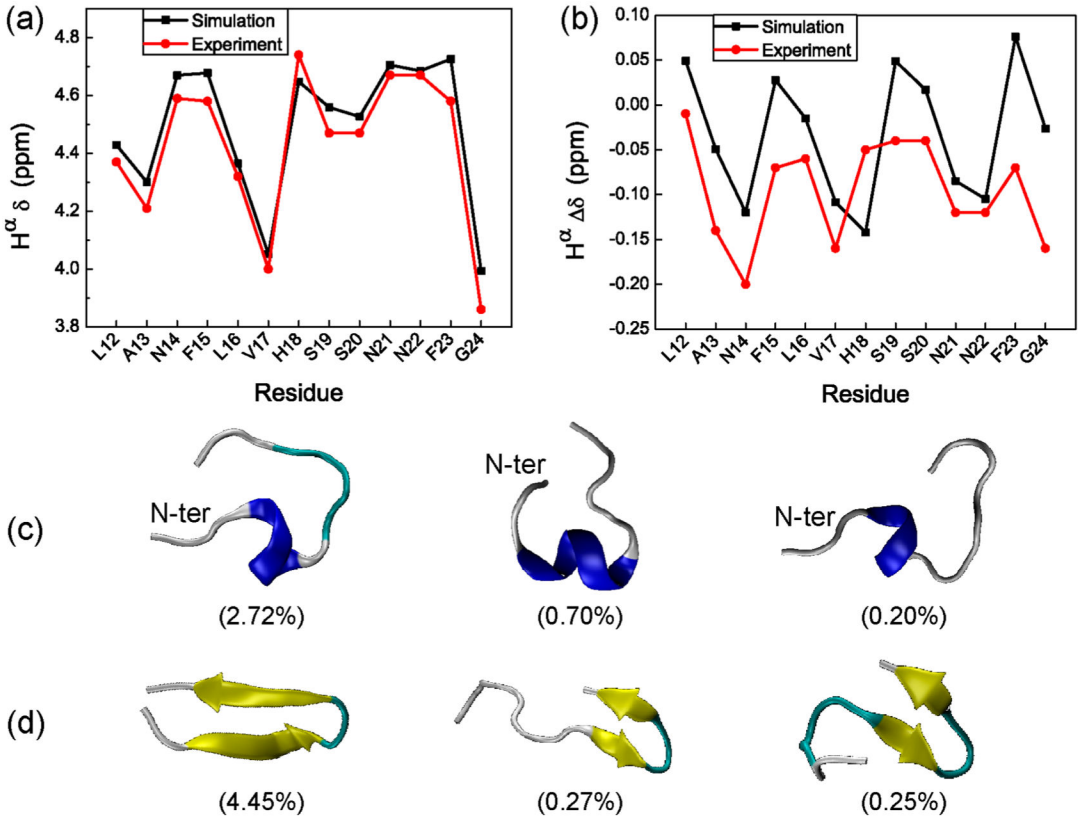

Figure 1.

Comparison between calculated and experimental chemical shifts of hIAPP(11–25) monomer along with representative REMD-generated α-helical and β-structures at 310 K. (a) H^{α} chemical shifts (δ), (b) H^{α} secondary chemical shifts ($\Delta\delta$), (c) three representative α-helical structures, and (d) three representative β-structures.

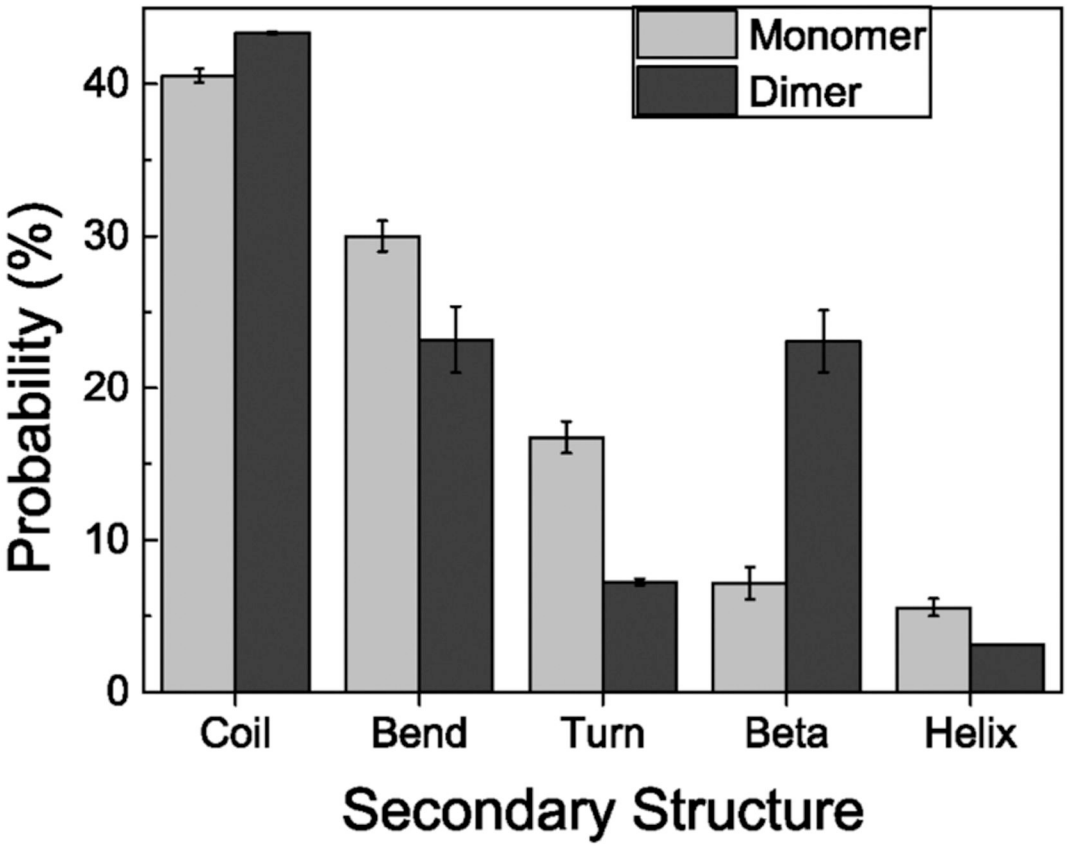

Figure 2.
Calculated secondary structure probabilities for monomers and dimers.

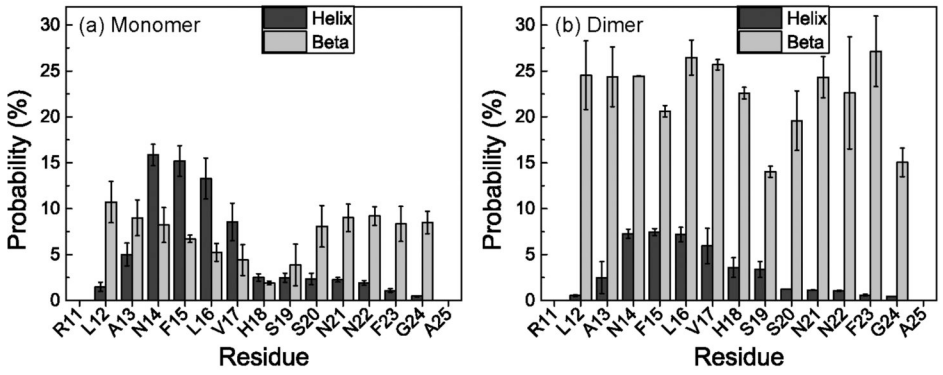

Figure 3.

Helix and β-sheet probability of each amino acid residue for hIAPP(11–25) (a) monomer and (b) dimer.

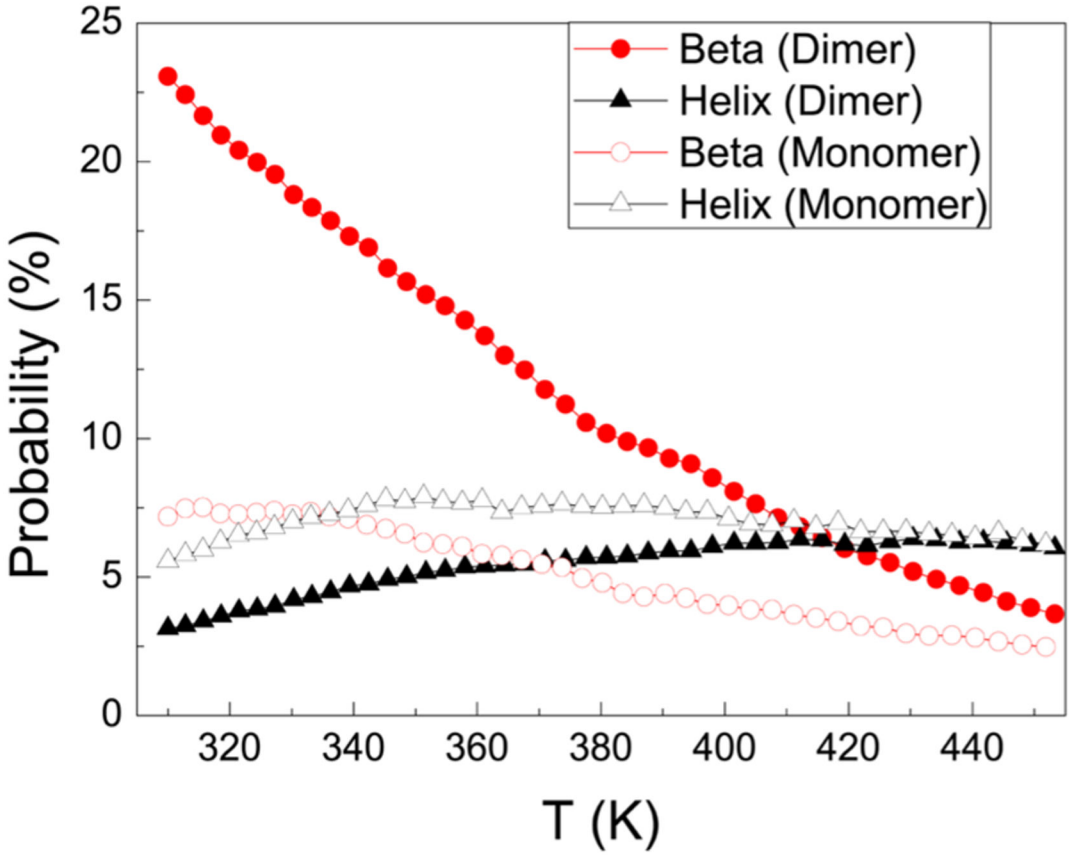

Figure 4.
Probability of helical and β structures as a function of temperature for hIAPP(11–25) monomer and dimer.

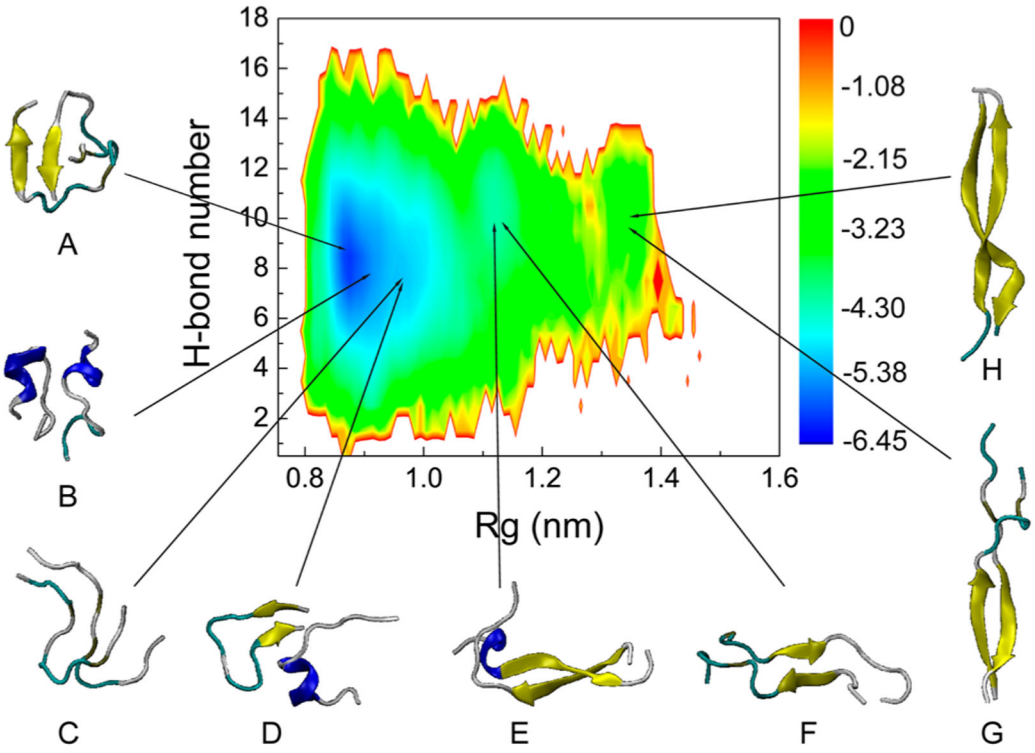

Figure 5.

Free energy surface (in kcal/mol) for the hIAPP(11–25) dimer at 310 K as a function of radius of gyration (R_g) and the total number of intra- and intermolecular H-bonds (H-bond number). The free energy surface contains three minimum energy basins, centered at (R_g, H-bond number) values of (0.85 nm, 8), (1.12 nm, 10), and (1.33 nm, 11). Representative structures in each minimum-energy basin are also given, along with their probabilities: 0.10% (A), 0.04% (B), 0.20% (C), 0.03% (D), 2.17% (E), 0.03% (F), 0.38% (G), and 0.35% (H).

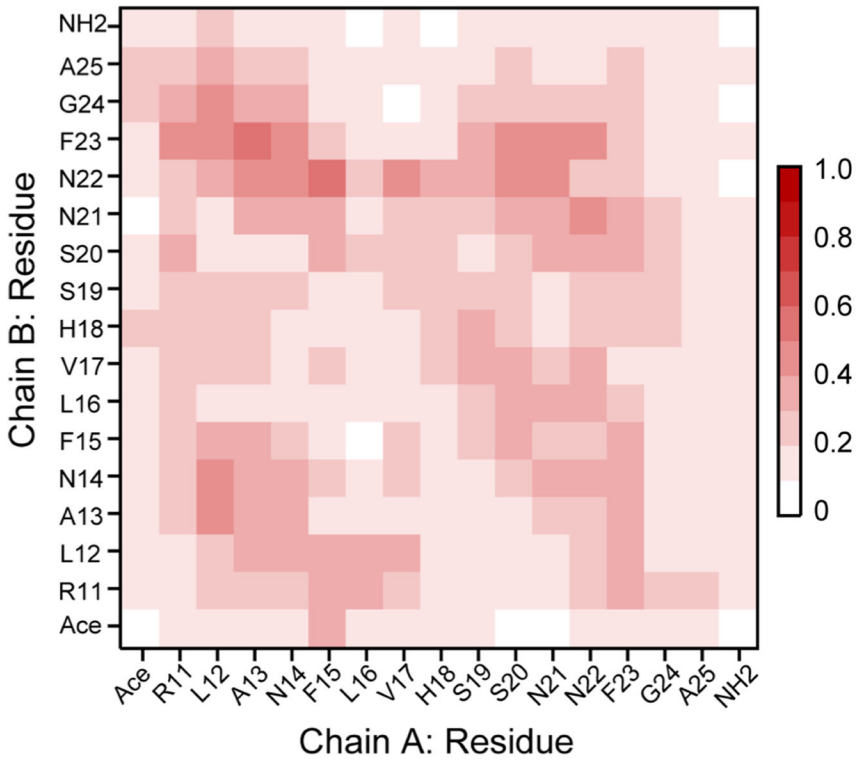

Figure 6.
REMD-generated peptide–peptide atomic contact probability map of hIAPP(11–25) dimer at 310 K.

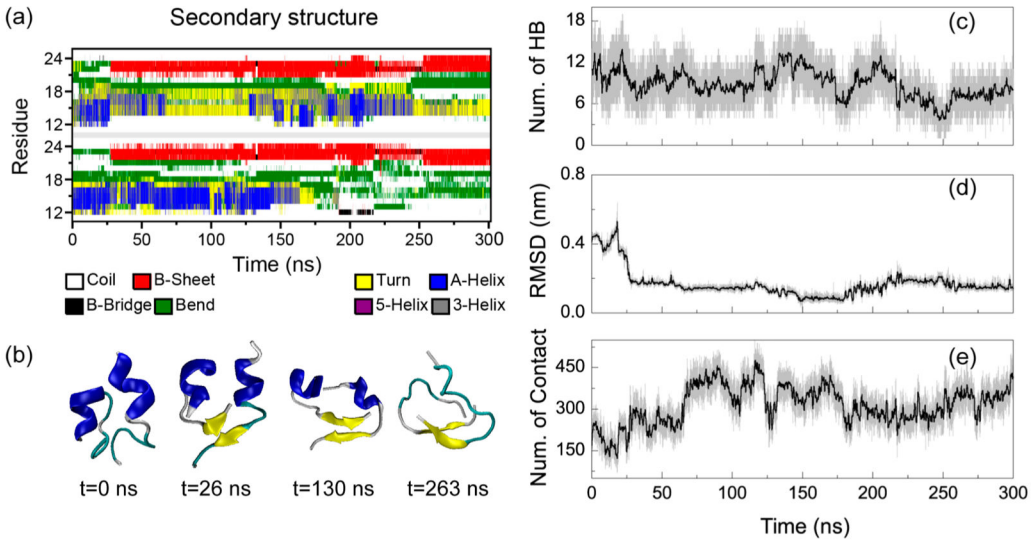

Figure 7.

Analysis of a representative helix-to-β-sheet transition pathway following mechanism I. (a) Secondary structure of each residue as a function of simulation time. (b) Four representative snapshots at 0, 26, 130, and 263 ns of the MD run. Time evolution of (c) number of main-chain H-bonds, (d) main-chain RMSD with respect to the short antiparallel β-sheet formed at t = 150 ns, and (e) number of interpeptide atomic contacts. The antiparallel β-sheet at t = 150 ns has a main-chain RMSD of 0.17 nm with respect to the snapshot at t = 263 ns. The black curve in (c)–(e) is a smoothed line over five data points.

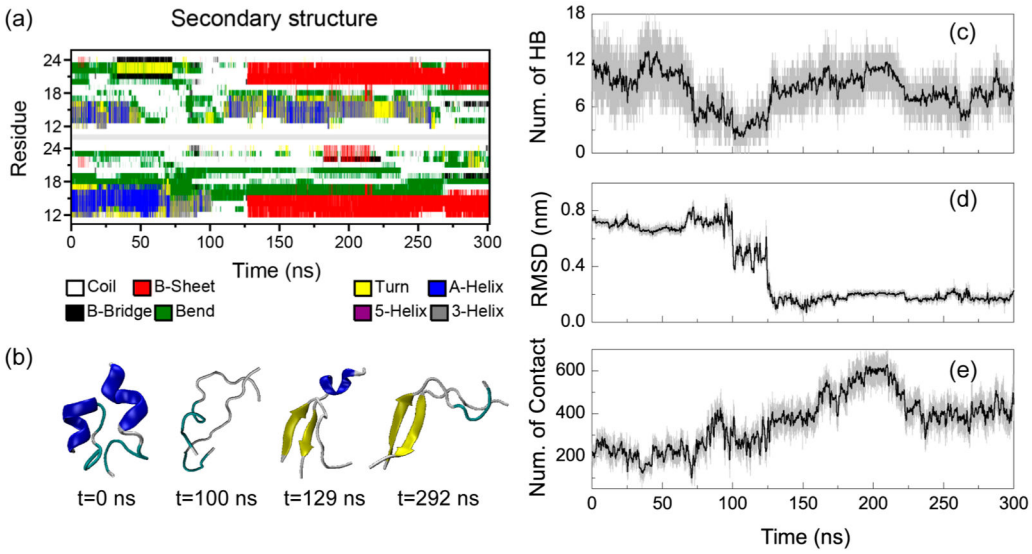

Figure 8.

Analysis of a representative helix-to-β-sheet transition pathway following mechanism II. (a) Secondary structure of each residue as a function of simulation time. (b) Four representative snapshots at 0, 100, and 292 ns of the MD run. Time evolution of (c) number of main-chain H-Bonds, (d) main-chain RMSD with respect to the short antiparallel β-sheet formed at t = 150 ns, and (e) number of interpeptide atomic contacts. The antiparallel β-sheet at t = 150 ns has a main-chain RMSD of 0.19 nm with respect to the snapshot at t = 292 ns. The black curve in (c)–(e) is a smoothed line over five data points.

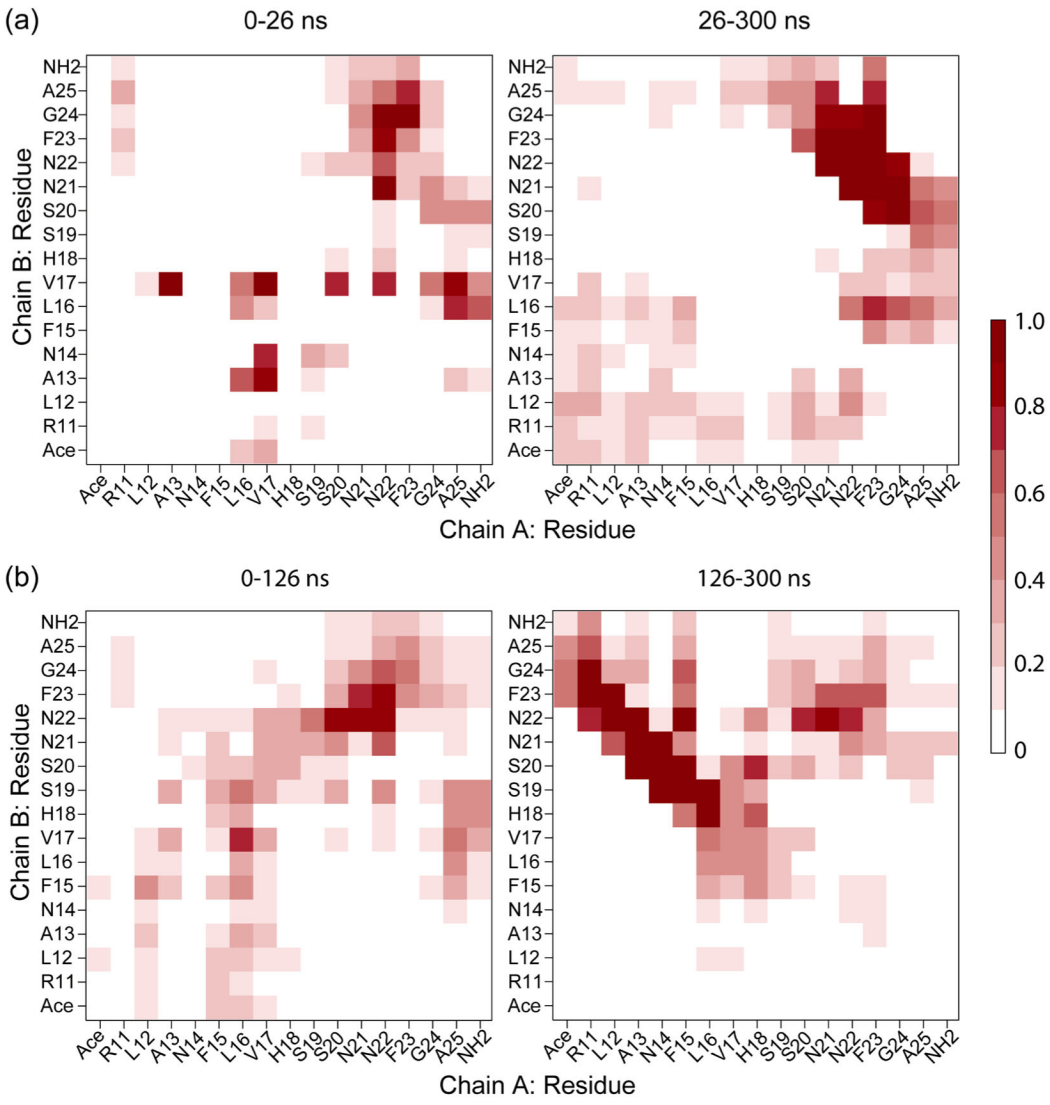

Figure 9.

MD-generated interpeptide contact probability map of hIAPP(11–25) dimer before (left panel) and after (right panel) β-sheet formation for (a) the MD run shown in Figure 7 and (b) the MD shown in Figure 8